



Late Cenozoic Denudation and Topographic Evolution History of the Lhasa River Drainage in Southern Tibetan Plateau: Insights From Inverse Thermal History Modeling

Dongxu Cai¹, Xianyan Wang^{1*}, Guangwei Li^{2*}, Wenbin Zhu² and Huayu Lu¹

¹ School of Geography and Ocean Science, Nanjing University, Nanjing, China, ² School of Earth Sciences and Engineering, Nanjing University, Nanjing, China

OPEN ACCESS

Edited by:

Gang Rao,
Zhejiang University, China

Reviewed by:

Jingen Dai,
China University of Geosciences,
China
Ruohong Jiao,
University of Victoria, Canada

*Correspondence:

Xianyan Wang
xianyanwang@nju.edu.cn
Guangwei Li
guangweili@nju.edu.cn

Specialty section:

This article was submitted to
Quaternary Science, Geomorphology
and Paleoenvironment,
a section of the journal
Frontiers in Earth Science

Received: 01 December 2020

Accepted: 09 March 2021

Published: 29 April 2021

Citation:

Cai D, Wang X, Li G, Zhu W and
Lu H (2021) Late Cenozoic
Denudation and Topographic
Evolution History of the Lhasa River
Drainage in Southern Tibetan Plateau:
Insights From Inverse Thermal History
Modeling. *Front. Earth Sci.* 9:636459.
doi: 10.3389/feart.2021.636459

The interaction of surface erosion (e.g., fluvial incision) and tectonic uplift shapes the landform in the Tibetan Plateau. The Lhasa River flows toward the southwest across the central Gangdese Mountains in the southern Tibetan Plateau, characterized by a low-relief and high-elevation landscape. However, the evolution of low-relief topography and the establishment of the Lhasa River remain highly under debate. Here, we collected thermochronological ages reported in the Lhasa River drainage, using a 3D thermokinematic model to invert both late Cenozoic denudation and relief history of the Lhasa River drainage. Our results show that the Lhasa River drainage underwent four-phase denudation history, including two-stage rapid denudation at ~25–16 Ma (with a rate of ~0.42 km/Ma) and ~16–12 Ma (with a rate of ~0.72 km/Ma). In the latest Oligocene–early Miocene, uplift of the Gangdese Mountains triggered the rapid denudation and the formation of the current main drainage of the Lhasa River. In the middle Miocene, the second stage of the rapid denudation and the high relief were associated with intense incision of the Lhasa River, which is probably due to the enhanced Asian summer monsoon precipitation. This later rapid episode was consistent with the records of regional main drainage systems. After ~12 Ma, the denudation rate decreases rapidly, and the relief of topography in the central Gangdese region was gradually subdued. This indicates that the fluvial erosion resulting from Asian monsoon precipitation increase significantly impacts on the topographic evolution in the central Gangdese region.

Keywords: tectonic geomorphology, low-temperature thermochronology, Lhasa River, Tibetan Plateau, thermokinematic modeling, relief development

INTRODUCTION

The landscape evolution of the orogenic belt results from the complex interaction between tectonic uplift and surface erosion (e.g., fluvial incision). However, surface erosion is also influenced by tectonic forcing and climatic change on the different temporal scales (Davis et al., 1983; England and Molnar, 1990; Whipple et al., 2000; Schildgen et al., 2009; Whipple, 2009). For example, the

tectonic uplift creates a topographic gradient that increases fluvial incision and triggers landslides (Ahnert, 1970; Wilson and Fowler, 2011; Wang et al., 2012; Tian et al., 2015). An intensified monsoon precipitation or increased amplitudes of glacial–interglacial climatic fluctuations could also enhance fluvial incision (Zhang et al., 2001; Pan et al., 2003; Clift et al., 2008; Wang et al., 2012, 2015; Nie et al., 2018), which may in turn have an impact on tectonic activity (Zeitler et al., 2001; Whipple, 2009). Thus, how tectonics, climate, and surface erosion are coupled to control the evolution of topography is a fundamental question.

The Tibetan Plateau, created by the India–Asia collision since the Cenozoic (Molnar et al., 2010), is a natural laboratory for examining the coupling of tectonics, climate, and erosion in shaping the landscape. Previous studies have important findings in the Himalayas (Beaumont et al., 2001; Bookhagen et al., 2005; Clift et al., 2008; Zhang et al., 2012) and the southern and southeastern Tibetan Plateau (Lang and Huntington, 2014; Liu-Zeng et al., 2018; Nie et al., 2018; Shen et al., 2019). However, these studies have not reached a consensus about the mechanism of the landscape evolution in some regions, such as the Gangdese region, a low-relief and high-elevation landscape in the southern Tibetan Plateau (**Figure 1**). In the Gangdese region, quantitative inversion of thermochronological ages of Gangdese batholith suggests a rapid exhumation stage from the Oligocene to the Miocene or ~ 22 –18 Ma due to the activity of the Gangdese Thrust system (Copeland et al., 1995; Yin et al., 1999; Dai et al., 2013). In contrast, other thermochronology studies suggest that the rapid denudation since ~ 23 or 20–10 Ma was linked to regional river incision or the intensification of the Asian monsoon (Li et al., 2016; Ge et al., 2017). Tremblay et al. (2015) indicated that a rapid exhumation stage at ~ 12 Ma has been interpreted as river incision in the Gangdese region. Thus, distinguishing the effects of regional tectonic, the fluvial incision, and intensification of the Asian monsoon on the landscape evolution of the central Gangdese region since the early Miocene remains the major ramifications.

The Lhasa River is one of the large rivers that cross the central Gangdese Mountains in southeastern Tibetan Plateau. The formation of the Lhasa River and its incision could influence on the evolution of low-relief landscape on the central Gangdese Mountains. However, the time of significant incision of the Lhasa River remains highly debated. One view indicates that the Lhasa River probably formed and incised before 80 Ma based on the age of sediment accumulation near Lhasa River outlet (Laskowski et al., 2019). The study of the evolution of the Yarlung River into which Lhasa flows suggests that the current Lhasa River possibly formed at 26–19 Ma (Wang et al., 2013; Li et al., 2017). Based on the numerical simulations and the inversion of thermochronological ages, Tremblay et al. (2015) believe that the current river in the southern Tibetan Plateau formed at ~ 12 –11 Ma. Thus, the timing of the Lhasa River initial flowing across the central Gangdese which could affect the landform evolution in this area is still unclear.

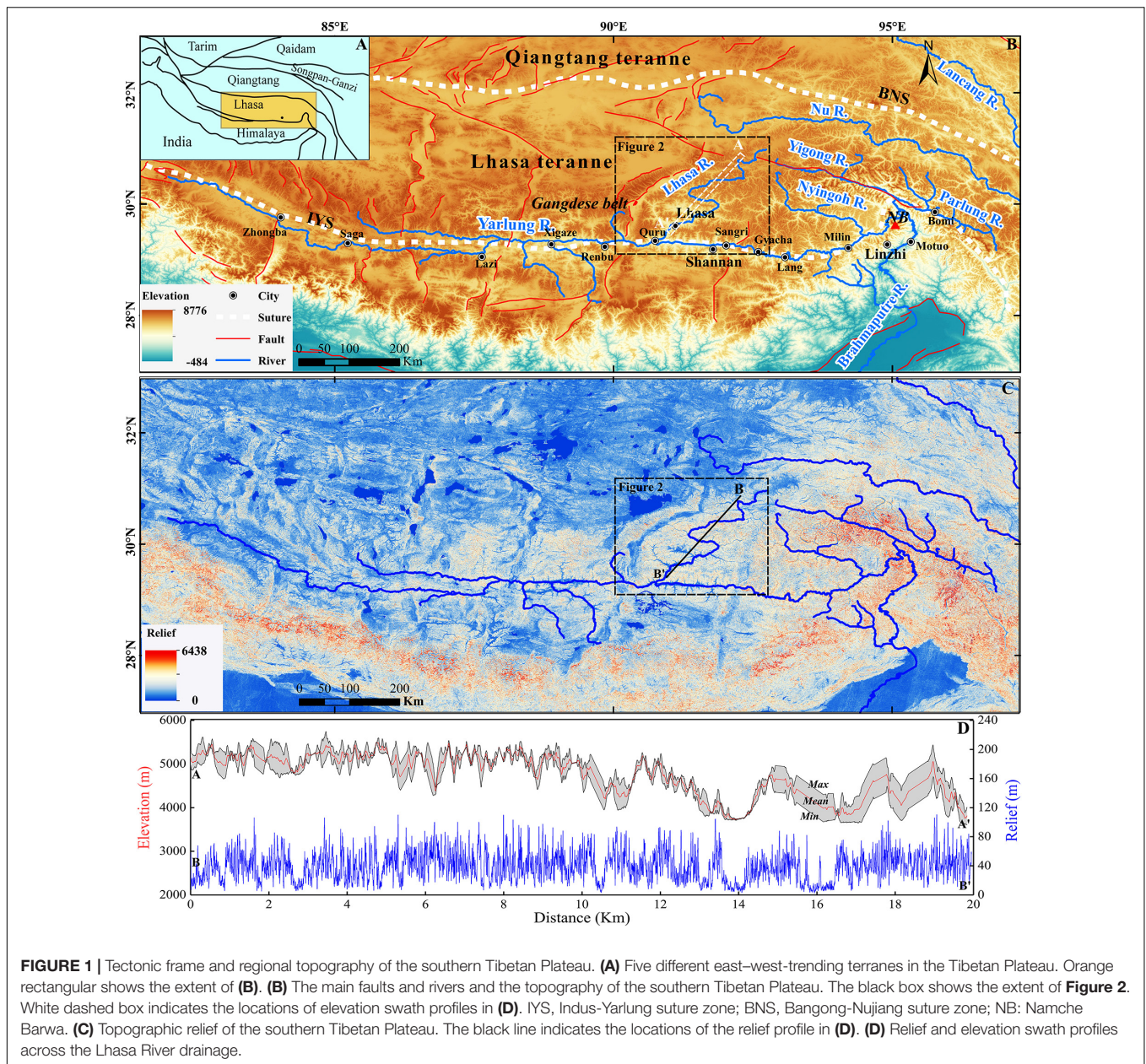
Low-temperature thermochronology may be able to provide information to solve this problem by carefully quantifying rates

and transition time of denudation of the Lhasa River drainage. However, previous studies in the Lhasa River drainage have only considered one-dimension cooling, neglecting potential effects of temporally varying topography and laterally varying denudation (Braun, 2002; Gallagher et al., 2005a,b; Luszczak et al., 2018). A numerical simulation method for inverse thermal history modeling, three-dimensional (3D) thermal kinematic model Pecube (Braun, 2002, 2003; Braun et al., 2012) coupled with the neighborhood algorithm (Sambridge, 2010a,b), has considered these limiting factors of one-dimension cooling. This method has been successfully applied to the inversion of denudation and topographic evolution in orogenic regions (Braun et al., 2012; Wang et al., 2016; McDannell et al., 2018; Shen et al., 2019; Yang et al., 2019). Here, we used this 3D thermokinematic modeling approach to invert both denudation and topographic evolution history in the Lhasa River drainage using low-temperature thermochronologic data from the Lhasa River Valley. The aims of this work are (i) to constrain the timing of the establishment of the modern Lhasa River and the evolution history of relatively low-relief topography in the southern Tibetan Plateau and (ii) to distinguish the respective roles that tectonics and climate played on the topographic evolution through numerical modeling of both thermal and relief histories in a drainage, using the Lhasa River drainage in the southern Tibetan Plateau as a case.

REGIONAL SETTING

The Cenozoic India–Asia collision created the high-elevation topography of the Tibetan Plateau, consisting of five different east–west-trending terranes, namely the Himalaya, Lhasa, Qiangtang, Songpan-Ganze, and Qaidam from south to north (Yin and Harrison, 2000; **Figure 1A**). The Lhasa terrane, located in the southern Tibetan Plateau, is bounded by the Bangong-Nujiang suture to the north and by the Indus-Yarlung suture to the south (Li et al., 2016). The Lhasa River headwaters originate in the eastern portion of the Lhasa terrane. The main trunk of the Lhasa River drains to the southwest across the Gangdese Mountains and merges into the east-flowing Yarlung River, forming a so-called barbed junction (**Figure 1B**). Our study area is located in the Lhasa River drainage within the Lhasa terrane (**Figure 1B**).

The extensive and widely exposed Late Triassic–Eocene Gangdese batholith intruded into the Paleozoic–Mesozoic sedimentary units in the study area (Ji et al., 2009; Zhu et al., 2011), which should record the later crustal thermal history. In the southern and central Lhasa River drainage, the Gangdese region exposes the lower Jurassic volcano-sedimentary sequence of the Yeba Group (Zhu et al., 2011), the lower Cretaceous volcanic rocks of the Sangri Group, and the Cretaceous–Tertiary volcanic rocks of the Linzizong Group (Mo et al., 2008; **Figure 2**). The widely distributed Paleozoic sedimentary strata in the Lhasa River drainage consist of Ordovician and Carboniferous to Cretaceous clastic sediments (Wei et al., 2014), and the middle–late Jurassic deposits mainly distribute on the upper reaches of Lhasa River. However, the Paleocene–Eocene sedimentary rocks in the Lhasa River drainage are limited or apparently

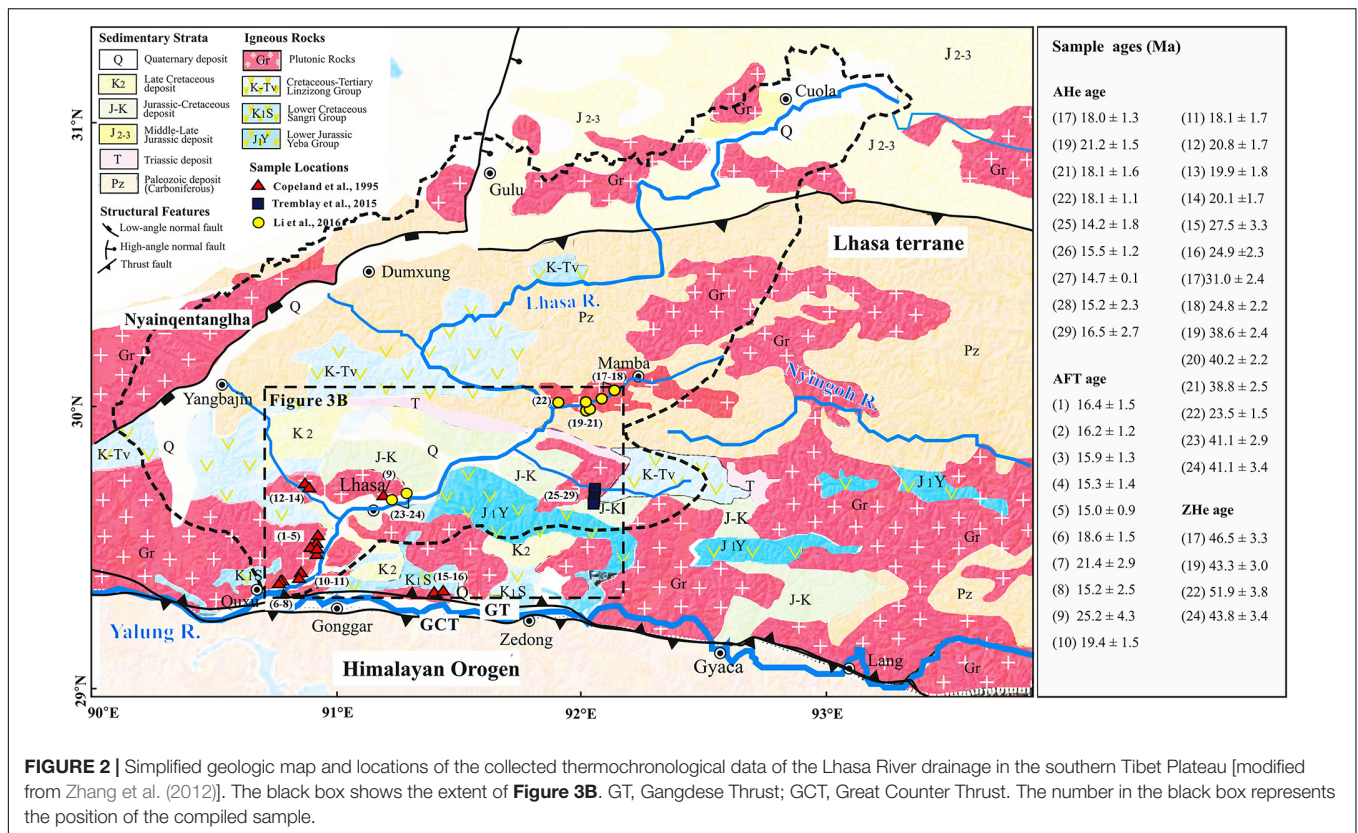


absent (Yin and Harrison, 2000). The Quaternary sediments expose along the lower reaches of the Lhasa River and the Rift valley (**Figure 2**).

The main faults in the study area since the Cenozoic include the Gangdese Thrust (GT), the Great Counter Thrust (GCT), and the north–south-trending normal fault (**Figure 2**). The north-dipping Gangdese Thrust activated between ~ 30 and 23 Ma and has an estimated 50–60 km of shortening along the Indus-Yarlung Zangpo suture zone (Yin et al., 1999; Wei et al., 2014). The south-dipping Great Counter Thrust juxtaposed the passive continental margin sediments of northern India over the Indus-Yarlung ophiolites (Yin et al., 1999; Li Y. L. et al., 2015). The isotopic dating of Gangdese batholith in southern Tibetan Plateau constrains that the activity of GCT was between ~ 25 and

10 Ma (Yin et al., 1999; Harrison et al., 2000). The north–south-trending Yangbajing-Yardong graben system developed during the late Miocene, which reflects the E–W extensional regime in the Tibetan Plateau (Harrison et al., 1992; Li Y. L. et al., 2015).

The climate in the Lhasa River drainage is substantially influenced by the South Asian summer monsoon (**Figure 1**). Global monsoon systems are generally considered to be associated with seasonal changes in the land–sea thermal contrast and the shift of Intertropical Convergence Zone (Gadgil, 2003; Wang et al., 2017). During the boreal summer when the sensible heating of the Asian continent by solar insolation is at a maximum, the Intertropical Convergence Zone is located over the Indian continent, where the SE trade winds in the Southern Hemisphere change direction to NE after crossing the equator



(Wang et al., 2017). The SE trade winds bring air masses carrying abundant moisture from the Bay of Bengal to the north and northwest (Bookhagen et al., 2005). When these vortexes encounter the frontal terrain of the Himalaya, they were released to produce a large amount of topographic precipitation, and only a small part of the water vapor can be transported further to high-altitude areas on the Tibetan Plateau through the valleys of the Himalayan transverse river (Bookhagen and Burbank, 2010). The precipitation of modern Lhasa River drainage do not exceed 500 mm (Bookhagen and Burbank, 2010).

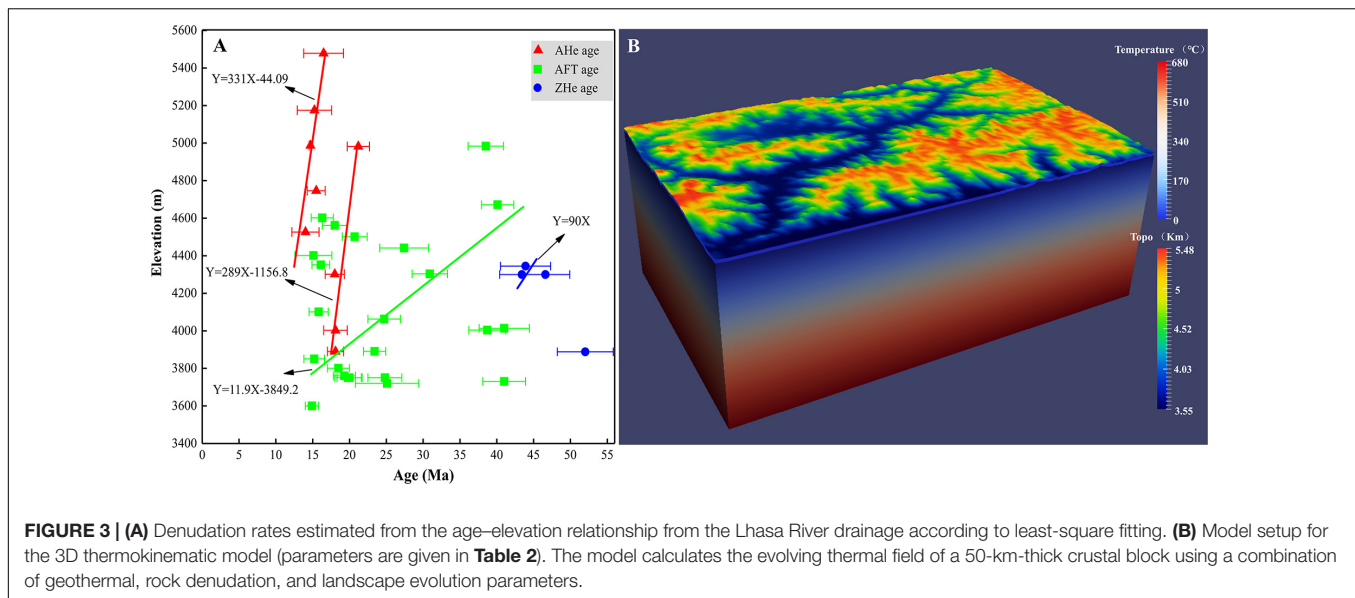
ANALYSIS METHODS

Data and Age–Elevation Relationship

In order to constrain the timing of rapid denudation of the Lhasa River, the published thermochronological ages in Lhasa River valley were compiled (**Figure 2**). This low-temperature thermochronological dataset includes 9 apatite (U-Th)/He (AHe) ages, 24 apatite fission-track (AFT) ages, and 4 zircon (U-Th)/He (ZHe) ages (Copeland et al., 1995; Tremblay et al., 2015; Li et al., 2016; **Figure 2** and **Supplementary Table 1**). Five AHe ages ranging from 14.2 ± 1.8 to 16.5 ± 2.7 Ma are from the middle reaches and along a 1.2-km elevation transect in the eastern tributary of the Lhasa River (Tremblay et al., 2015), and four AHe ages ranging from 18.0 ± 1.3 to 21.2 ± 1.5 Ma are from the eastern tributary valley of the Lhasa River (Li et al., 2016; **Figure 2** and **Supplementary Table 1**). AFT ages,

ranging between 15.0 ± 0.9 and 41.1 ± 3.4 Ma, are mainly from the middle and lower reaches of the Lhasa River valley, but two are from the Yarlung River valley (**Figure 2** and **Supplementary Table 1**). ZHe ages, ranging between 43 ± 3.0 and 51.9 ± 3.8 Ma, are from the valley-wall transects in the middle and lower reaches of the Lhasa River (Li et al., 2016; **Figure 2** and **Supplementary Table 1**). However, six ZHe ages from the tributary of Lhasa River reported in Tremblay et al. (2015) are much younger than the ZHe and AFT and AHe ages in the region reported in Copeland et al. (1995) and Li et al. (2016). This is probably caused by the locally structural/thermal effect. In order to avoid the uncertainty, these data are not selected. All thermochronological ages, at elevation between 3,600 and 5,478 m, were collected from Mesozoic and Early Cenozoic Gangdese batholith granites.

In order to provide first-order estimates of the denudation parameters in Pecube, the age–elevation relationship (AER) was plotted from thermochronological data from river valleys. Here, we assume that the Lhasa River drainage underwent the history of uniform denudation in space, and then the variable slopes of the different AERs can be interpreted as reflecting a change in the denudation rate of this region (Gallagher et al., 2005a,b; Beek et al., 2010). The ZHe data suggest a relatively rapid denudation rate of 0.09 km/Ma between ~ 47 and ~ 43 Ma, but a lower rate of 0.01 km/Ma between ~ 43 and ~ 15 Ma from the AFT data (**Figure 3A**). The steeper age–elevation relationship from AHe data implies an increase in regional denudation rates to ~ 0.289 km/Ma from ~ 23 to ~ 16 Ma and ~ 0.331 km/Ma between



~16 and ~12 Ma (**Figure 3A**). Varying denudation rates are also suggested by the AFT data, which indicates a rapid denudation phase at around ~23 Ma. These data were used to set the possible variation range of the parameters in the modeling (see details in the following).

In fact, the estimation from the AER is simply one-dimensional, which possibly under- or overestimates the denudation rate (Braun et al., 2012), because of neglecting the possible effects of temporally varying topography on underlying isotherms, and/or neglecting possible effects of relief development. Moreover, the internal consistency between the different datasets and their inferred interpretation has not been assessed. Thus, we will analyze these data using Pecube (Braun et al., 2012) to more quantitatively infer the denudation and relief history of Lhasa River drainage.

Thermokinematic Modeling

Pecube is a finite-element thermokinematic modeling that solves the 3D heat transport equation (Braun, 2003):

$$\rho c \left(\frac{\partial T}{\partial t} + v \frac{\partial T}{\partial z} \right) = \frac{\partial}{\partial x} k \frac{\partial T}{\partial x} + \frac{\partial}{\partial y} k \frac{\partial T}{\partial y} + \frac{\partial}{\partial z} k \frac{\partial T}{\partial z} + H \quad (1)$$

where $T(x,y,z,t)$ is the temperature ($^{\circ}\text{C}$), ρ is the rock density (kg/m^3), c is the heat capacity ($\text{J}/\text{kg}/\text{K}$), v is the vertical velocity of the rock particle relative to the base of the crust (km/Ma), k denotes conductivity ($\text{W}/\text{m}/\text{k}$), and H is the radioactive heat production (W/m^3). In a crustal block, the thermal properties such as rock conductivity, heat capacity, density, and heat production were assumed to remain constant through time, and then Eq. (1) was solved to reflect a crustal block undergoing lateral and vertical rock particle transport, denudation, and surface change. The surface change is incorporated here using the relief factor R , defined as the ratio between the relief amplitude (Δh_i) when rocks passed through the closure isotherms and the modern-day relief amplitude

(Δh_0) (Valla et al., 2010):

$$R = \frac{\Delta h_i}{\Delta h_0} \quad (2)$$

when $R = 0$, the initial topography is a plateau at the maximum present-day elevation; when $R = 1$, the paleo-relief was the same as the modern topography; for $R < 1$, the paleo-relief is lower than today, while for $R > 1$, the paleo-relief is higher than today.

During a Pecube model inversion, a two-step neighborhood algorithm was used (Sambridge, 2010a,b). The first step involves an iterative search in the multidimensional parameter space in order to find sets of input parameters that minimize the misfit between observed and predicted data. The misfit was calculated as

$$m = \frac{1}{n} \sqrt{\sum_{i=1}^n \frac{(p_i - o_i)^2}{\sigma_i^2}} \quad (3)$$

where m is the misfit value; n is the number observed data; and for each data point i , is the age predicted by Pecube; o_i and σ_i are the observed age and its error, respectively. The second step of the neighborhood algorithm is an appraisal of the search results to define statistical limits on the ranges of input parameters that provide a good fit to the observed age data (Sambridge, 2010b), and Bayesian inference is used to produce posterior probability density functions (PPDFs) for each individual parameter using a likelihood function L ,

$$L = \exp \left(-\frac{n}{2} \sqrt{\sum_{i=1}^n \frac{(p_i - o_i)^2}{\sigma_i^2}} \right) \quad (4)$$

The appraisal yields 1D and 2D PPDFs for the model parameters that are presented for each set of model parameters in **Table 1**.

The input thermokinematic parameters used in Pecube are listed in **Table 2**. We set a 50-km depth model, and the basal

TABLE 1 | Values of parameters of input and inversion results.

Parameters	Denudation (three-phase)		Denudation (four-phase)		Denudation (five-phase)		Relief scenario	
	Range	Best-fit parameter	Range	Best-fit parameter	Range	Best-fit parameter	Range	Best-fit parameter
Basal temperature (°C)	500–1,000	665	500–1,000	646	500–1,000	617	646	–
R	0–2	0.61	0–2	0.38	0–2	0.9	0–1.5	0.49
T1 (Ma)	30–10	16	30–20	24.6	40–30	31.5	24.6	–
E1 (km/Ma)	0–1.5	0.29	0–1.5	0.07	0–1.5	0.09	0–1.5	0.09
R1	–	–	–	–	–	–	0–2	0.85
T2 (Ma)	20–10	12.1	25–15	15.5	30–20	23.8	15.5	–
E2 (km/Ma)	0–2	1.75	0–2	0.39	0–1.5	0.02	0–2	0.42
R2	–	–	–	–	–	–	0–2	0.82
T3 (Ma)	0	0	15–10	12.3	25–15	17.2	12.3	–
E3 (km/Ma)	0–2	0.18	0–2	1.22	0–2	0.41	0–2	0.72
R3	–	–	–	–	–	–	0–2	1.58
T4 (Ma)	–	–	0	0	15–10	13.3	0	–
E4 (km/Ma)	–	–	0–2	0.08	0–2	0.71	0–2	0.16
T5 (Ma)	–	–	–	–	–	0	–	–
E5 (km/Ma)	–	–	–	–	0–2	0.22	–	–
Number of models	7,100	–	7,100	–	10,800	–	10,800	–
Free parameters	7	–	9	–	11	–	8	–
Resample rate	71%	–	71%	–	90%	–	90%	–
Misfit	–	0.74	–	0.35	–	0.40	–	0.35

Notes: T1, T2, T3, and T4 represent the first, second, third, and fourth transition time, respectively; E1, E2, E3, E4, and E5 represent the denudation rate of the first, second, third, fourth, and fifth phase, respectively; R, R1, R2, and R3 represent the topographic relief of the initial, first, second, and third transition time, respectively.

temperature of the model is a free parameter ranging between 500 and 1,000°C, which is equivalent to an initial geothermal gradient of ~10–20°C/km. The initial geothermal gradient in the Lhasa River drainage should be lower than the present-day (~20–30°C/km), because the late Cenozoic denudation should have increased the thermal gradient to the current values (Ehlers, 2005). The starting time of the model was set as 41 Ma, as the reported oldest thermochronological age in the main trunk of the Lhasa River valley is ~41 Ma. Cenozoic faults are absent within the selected simulation area (Figure 2); thus, the faults are not considered in our model. The geometry of the surface topography was extracted from 90-m resolution DEMs (Figure 3B).

TABLE 2 | Thermokinematic and elastic parameters used in this study.

Parameter name	Parameter range	Units	Reference
Thermal conductivity	2.5	W/m/K	Whipp et al. (2007)
Crustal density	2,700	kg/m ³	
Thermal diffusivity	25	km ² /My	
Mean annual surface temperature	15	°C	
Atmospheric lapse rate	6	°C/km	Naito et al. (2006)
Model time step	Optional	years	
Basal temperature	500–1,000	°C	
Horizontal node spacing	0.9	km	
Vertical node spacing	0.9	km	
Model domain	140 × 90 × 50	km	
Model starting time	41	Ma	

In order to obtain a more robust and detailed view of the denudation rate, transition time, and topographical relief in the Lhasa River drainage, two scenarios were modeled as the “denudation scenario” and the “relief scenario.” Here, we defined the “denudation scenario” as a steady evolution of topography scenario considering only spatially and temporally varying rock denudation rates, without considering the complex evolution of topography, and the initial topography changes linearly through time to modern. Based on previous studies for the denudation history in the Gangdese region, we have known apparently more than two-stage denudation history since 41 Ma in the Lhasa River drainage (Li et al., 2016). Thus, the assumption of three-phase, four-phase, and five-phase denudation history in the “denudation scenario” since 41 Ma was tested, respectively.

The inverted parameters are preliminarily set based on the AER, including the slope of AHe and AFT ages with uncertainty (Figure 3A). The parameters of the three-phase denudation history include (1) first and second transition time (T1, 30–10 Ma, and T2, 20–10 Ma, the reference basis for boundary setting shown in Supplementary Table 2); (2) denudation rates of the first, second, and third phase (E1 = 0–1.5 km/Ma, E2 = E3 = 0–2 km/Ma, referring from the slope of AHe and AFT in AER); and (3) initial relief (R, 0–2). The parameters of the four-phase denudation history include (1) first, second, and third transition time (T1, 30–20 Ma; T2, 25–15 Ma; and T3, 15–10 Ma); (2) denudation rates of the first, second, third, and fourth phase (E1 = 0–1.5 km/Ma; E2 = E3 = E4 = 0–2 km/Ma); and (3) initial relief (R, 0–2). For the five-phase denudation history, the parameters include (1) first, second, third, and fourth transition time (T1, 40–30 Ma; T2, 30–20 Ma; T3, 25–15 Ma; and T4,

15–10 Ma); (2) denudation rates of the first, second, third, fourth, and fifth phase ($E1 = E2 = 0\text{--}1.5$ km/Ma; $E3 = E4 = E5 = 0\text{--}2$ km/Ma); and (3) initial relief ($R, 0\text{--}2$).

The incision of the Lhasa River will affect the topographical relief. We also define a “relief scenario” to consider not only spatially and temporally varying rock denudation rates, but also the multistage evolution of topography due to the impact of the fluvial incision. The detailed parameters of this scenario were set according to the results of the “denudation scenario,” including four-phase denudation and topographic evolution history (Table 1, see section “denudation Scenario” for details). Inverted parameters of this scenario include the following: (1) the first, second, and third transition time set as 24.6, 15.5, and 12.3 Ma, respectively, according to the simulation result of the four-stage denudation in the “denudation scenario”; (2) the range of denudation rates of the first, second, third, and fourth phase, which are the same as four-phase denudation history in the “denudation scenario”; and (3) topographic relief of the initial, first, second, and third transition time ($R = R1 = 0\text{--}1.5$, $R2 = R3 = 0\text{--}2$). The input parameters of the modeling under different denudation stages and different scenarios are shown in Table 1.

MODELING RESULTS

Denudation Scenario

The results for best fitting of the three-phase denudation are shown in Table 1. We found the slow denudation at a rate of 0.29 km/Ma from 41 to 16 Ma, the rapid denudation at a rate of 1.75 km/Ma between 16 and 12 Ma, and a slow rate of 0.18 km/Ma since ~12 Ma (Table 1 and Supplementary Figure 1). However, a rapid phase of denudation since ~23 Ma reported by Li et al. (2016) is not reproduced in this modeling. For the inversion of five-phase denudation history, the denudation rates of best fitting of the first phase (a rate of 0.09 km/Ma from ~41 to 31.5 Ma) and second phase (a rate of 0.02 km/Ma from ~31.5 to 23.8 Ma) are not more than 0.1 km/Ma (Table 1 and Supplementary Figure 2), which can be considered as a slow denudation phase. Moreover, the minimum misfit value of the forward result for the three-phase and five-phase denudation history is 0.74 and 0.40, respectively, which is higher than the four-phase denudation history (0.35) (Table 1). Therefore, the assumption of four-phase denudation is much more possible for the Lhasa River drainage since 41 Ma.

The results for the inversion of four-phase denudation are shown in Figure 4. The best-fitting model shows that the transition time of four-phase denudation is 24.6, 15.5, and 12.3 Ma, respectively. The slow denudation phases are the episode between ~40 and 24.6 Ma with a rate of 0.07 km/Ma and the episode of ~12 Ma to the present with a rate of 0.08 km/Ma. The rapid denudation rates were the second and third phases that were 0.39 km/Ma from 24.6 to 15.5 Ma and 1.22 km/Ma from 15.5 to 12.3 Ma. Note that 1.22 km/Ma from 15.5 to 12.3 Ma from the modeled denudation rate was higher. The age of the best-fit forward model in this scenario is also basically close to the observed age, except that ZHe is slightly younger (Figure 5A).

Relief Scenario

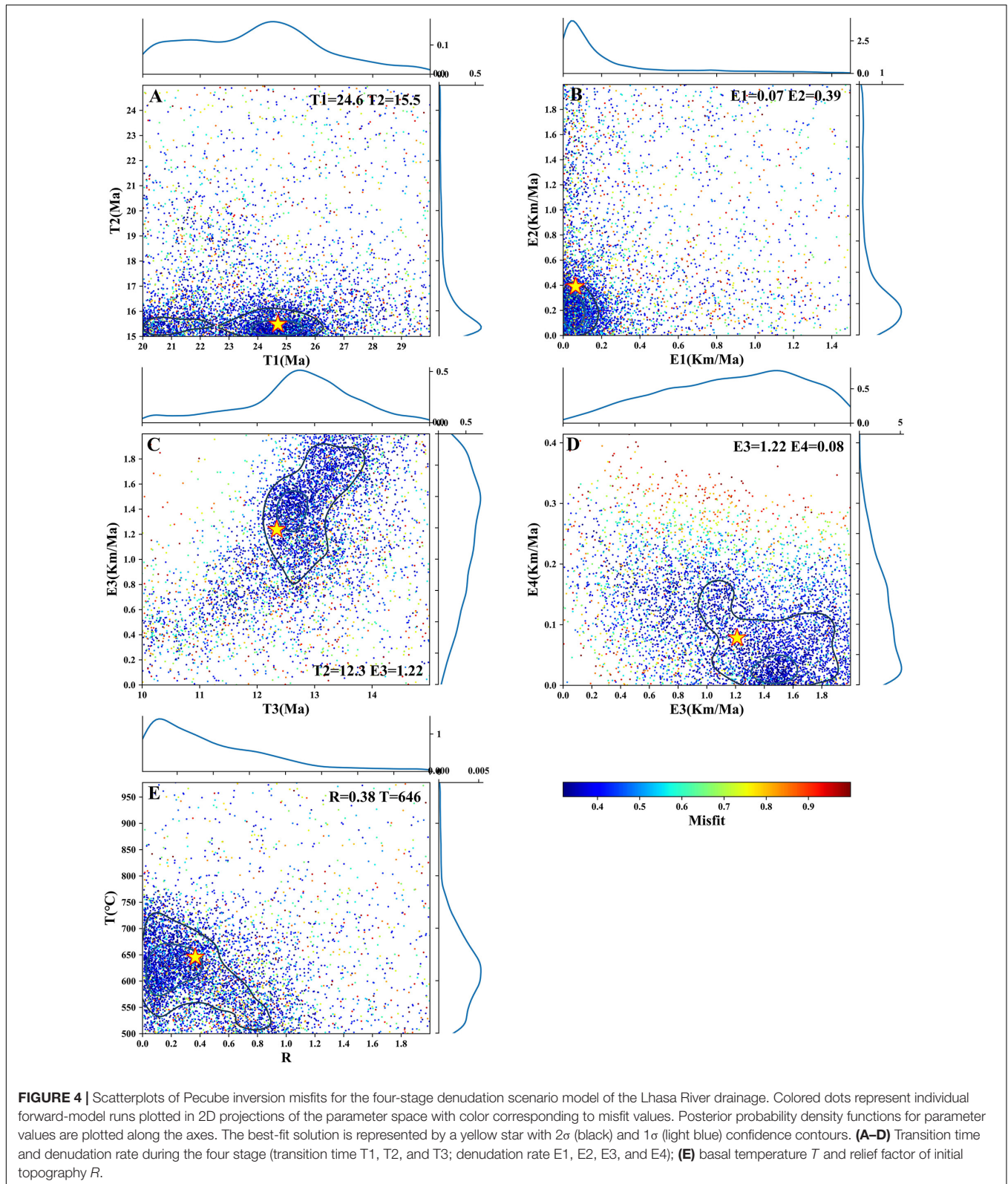
The incision of the Lhasa River valley leads to rapid denudation and changes in topographic relief. However, the simulation of the denudation scenario only inverted the initial relief. Therefore, we set the topography scenario with three additional relief parameters to invert the change of denudation rates and the evolution of topographic relief under the four-phase denudation (Table 1). The best-fitting model shows that the denudation rate of the four phases was 0.09, 0.42, 0.72, and 0.16 km/Ma, respectively (Figure 6). The denudation rate of the third stage in the relief scenario was lower than that of the denudation scenario, and the denudation rate in the other stages is close to the denudation scenario. The best fitting of the relief factor was 0.49 at 41 Ma, 0.85 at 24.6 Ma, 0.82 at 15.5 Ma, and 1.58 at 12.3 Ma, respectively. The relief factors at 41 and 25 Ma are not well converging and their errors are relatively large (Figures 6, 7), but the obvious changes in the relief after ~25 Ma have been well constrained (Figure 6). All ages of forwarding simulation under the relief scenario are basically consistent with the observed ages (Figure 5B).

DISCUSSION

The Timing of Establishment of the Modern Lhasa River

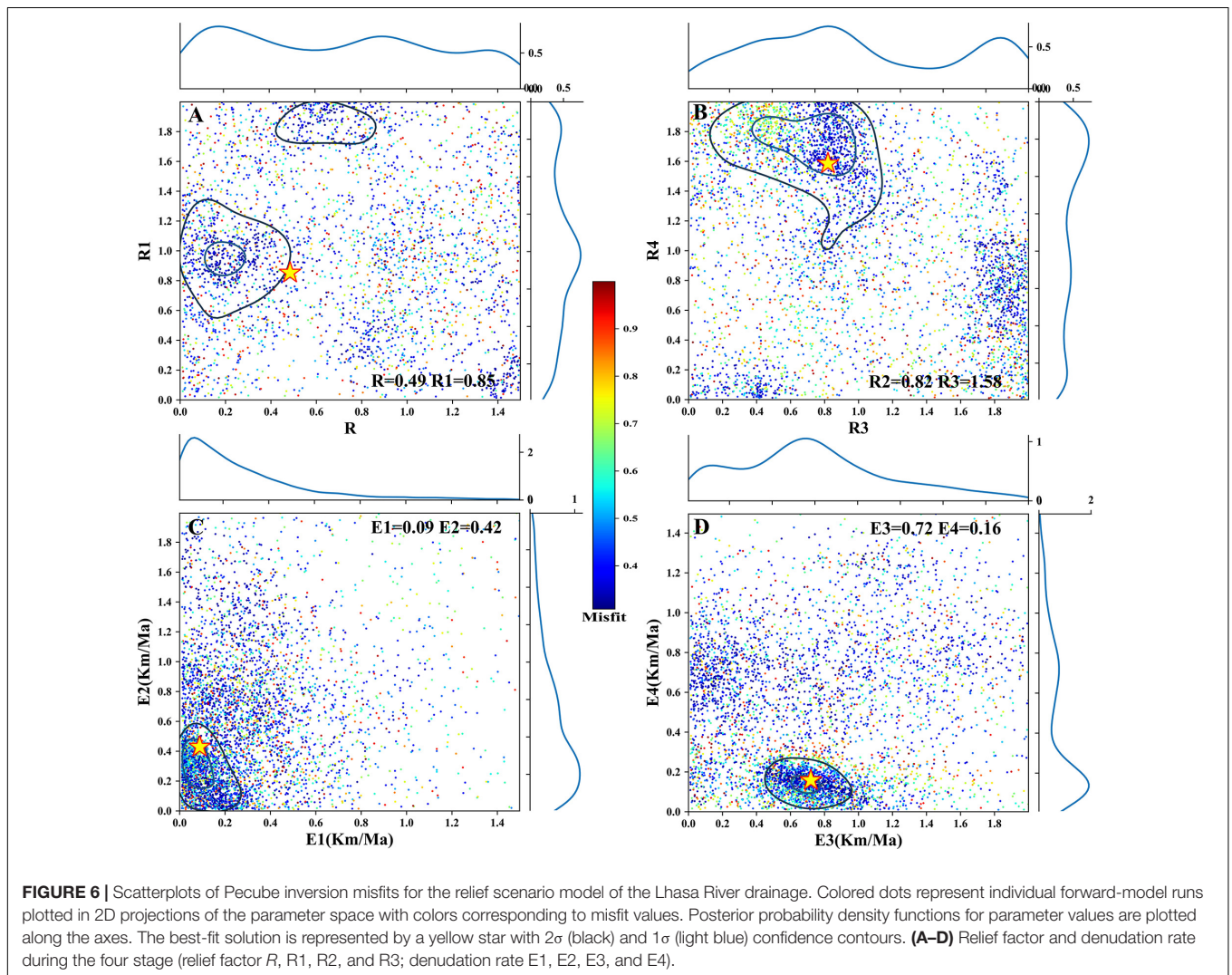
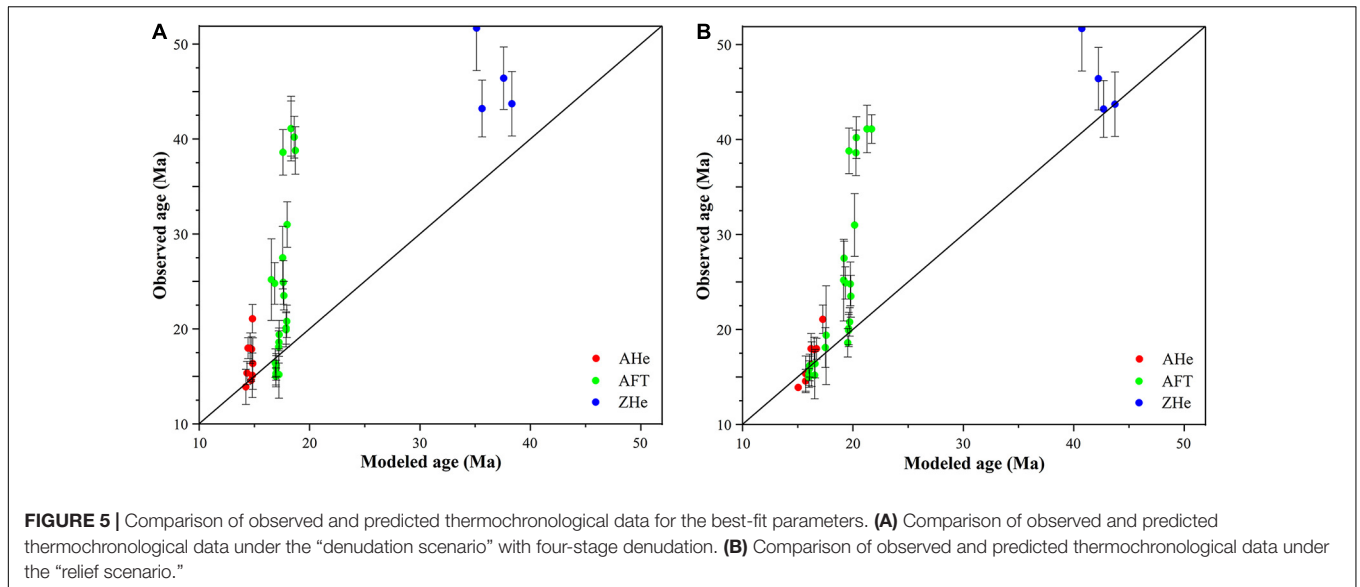
In this study, we found that the thermochronological ages in the main trunk are 41–14 Ma according to published thermochronological ages. The denudation history result of the modeling shows that rapid denudation started at ~25 Ma (Table 1 and Figure 4). The establishment of rivers will definitely cause rapid denudation of the valley. Of course, other factors such as increased tectonic uplift and rainfall and related discharge could also lead to the enhancement of river incision and rapid denudation. However, we suggest that the rapid denudation of the Lhasa River valley before 25 Ma may be also recorded by thermochronological data if the modern Lhasa River exists before 25 Ma. In fact, we only found that the rapid denudation of the Lhasa River valley started at ~25 Ma, probably suggesting that the modern Lhasa River in its modern extent did not exist prior to 25 Ma. In addition, the paleoaltimetric studies (e.g., carbon and oxygen stable isotopes) suggest that the northern portion of the Lhasa terrane where the Lhasa River originates was uplifted to near-modern elevations since around 25–23 Ma or much earlier (Rowley and Currie, 2006; DeCelles et al., 2007; Tian et al., 2013; Ding et al., 2014). If the Lhasa River did not start to develop at ~25 Ma, the rapid denudation might imply that the northern Lhasa terrane must have the rapid rock uplift, and thus, it can maintain the current elevation. However, the northern Lhasa terrane did not undergo rapid rock uplift since the late Oligocene (Hetzl et al., 2011; Li et al., 2016), which suggested that this rapid denudation episode is most likely associated with the initial incision of the upper reaches of the Lhasa River.

In addition, the main trunk of the Lhasa River drains to the southwest across the Gangdese Mountains and merges



into the Yarlung River (**Figure 1B**). Gangdese conglomerates are exposed discontinuously along the Yarlung River, and the depositional age of the Gangdese conglomerates is

26–23 Ma in the Xigaze forearc basin near the Lhasa River outlet (Wang et al., 2013; Carrapa et al., 2014). Paleocurrent measurements and provenance data indicate that the initial

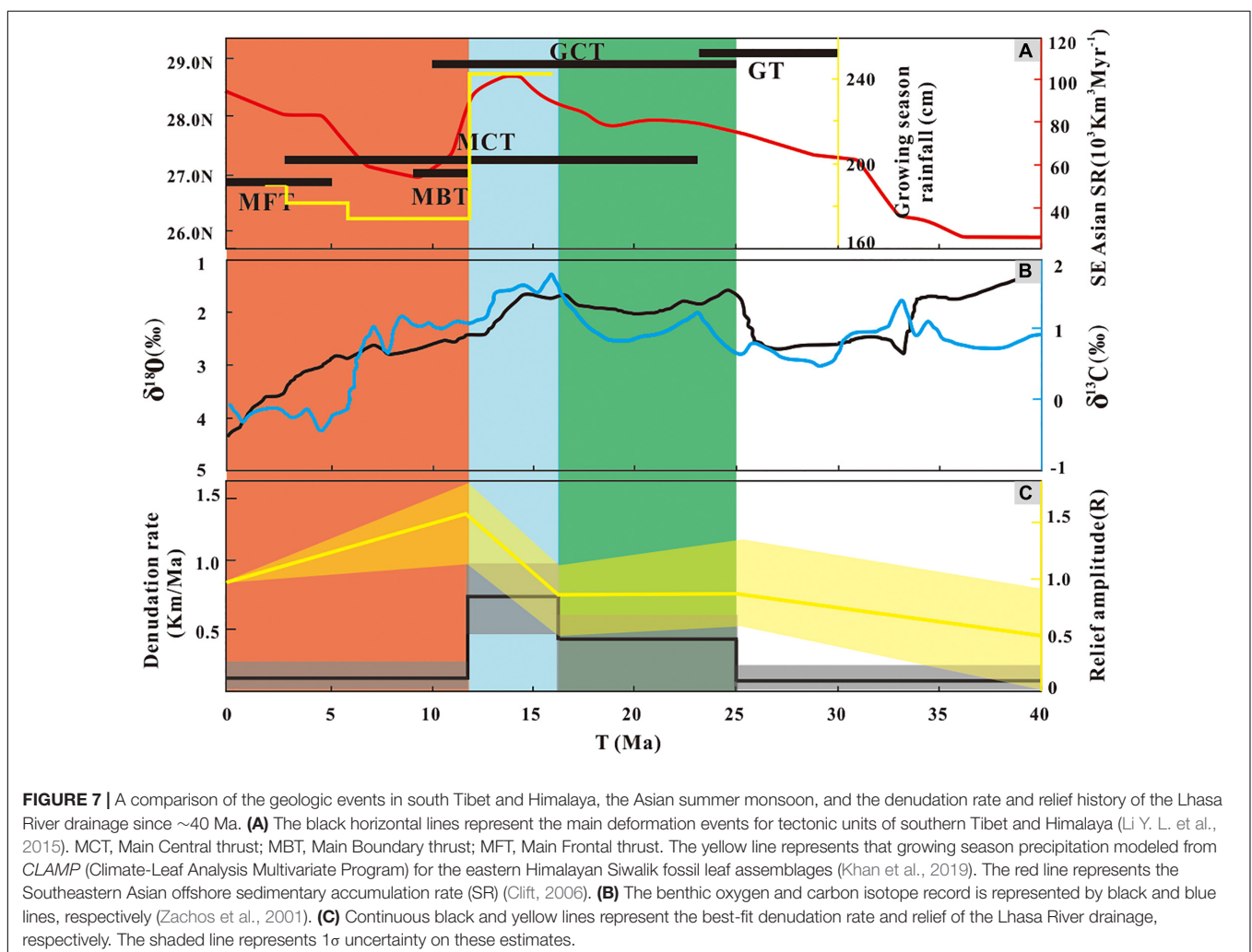


detritus of the Gangdese conglomerates were entirely derived from the north (mainly from the Gangdese arc) (Wang et al., 2013; Li et al., 2017), suggesting that the southward-draining relatively large rivers existed in the Gangdese region at least before ~23 Ma, and a large amount of material from the Gangdese arc can be transported southward. Furthermore, Laskowski et al. (2019) proposed that the paleo-Lhasa River may form since the Late Cretaceous based on the sedimentary provenance analysis. However, Li et al. (2018) summarized the incision history of modern tributaries of the Yarlung River and showed that tributaries on the north side of the Yarlung River (originating from the Lhasa terrane, including the Lhasa River) have only recorded progressively northward cooling episodes since the early Miocene. This could also verify the result of thermal history modeling. The southward-draining paleo-Lhasa River proposed by Laskowski et al. (2019) probably did not follow the current Lhasa River channel. In summary, according to these thermochronological, sedimentological, and paleoaltimetric evidence, the modern Lhasa River was probably established during the latest Oligocene–earliest Miocene.

Forcing for the Late Cenozoic Denudation and Topographic Evolution of Lhasa River Drainage

The Latest Oligocene–Early Miocene

Our best-fit model shows that the Lhasa River drainage underwent a rapid denudation from 24.6 to 15.5 Ma (with a rate of 0.42 km/Ma) (Figure 7C). The onset of rapid denudation occurred slightly earlier compared with the previous reported rapid exhumation timing (~23 or 20–10 Ma) (Li et al., 2016; Ge et al., 2017). The topographic relief did not change significantly with the increase of denudation during this stage (Figure 7C), suggesting a possible overall uplift in a large area including the Lhasa River drainage during this phase. The Gangdese Thrust is a north-dipping fault developed at the southern margin of the Lhasa River drainage (Figure 2), and it was active during late Oligocene–early Miocene (Yin et al., 1994; Li G. W. et al., 2015). Thus, the rapid denudation and relatively stable relief in this stage are most likely associated with the activity of the Gangdese Thrust (Figure 7A).



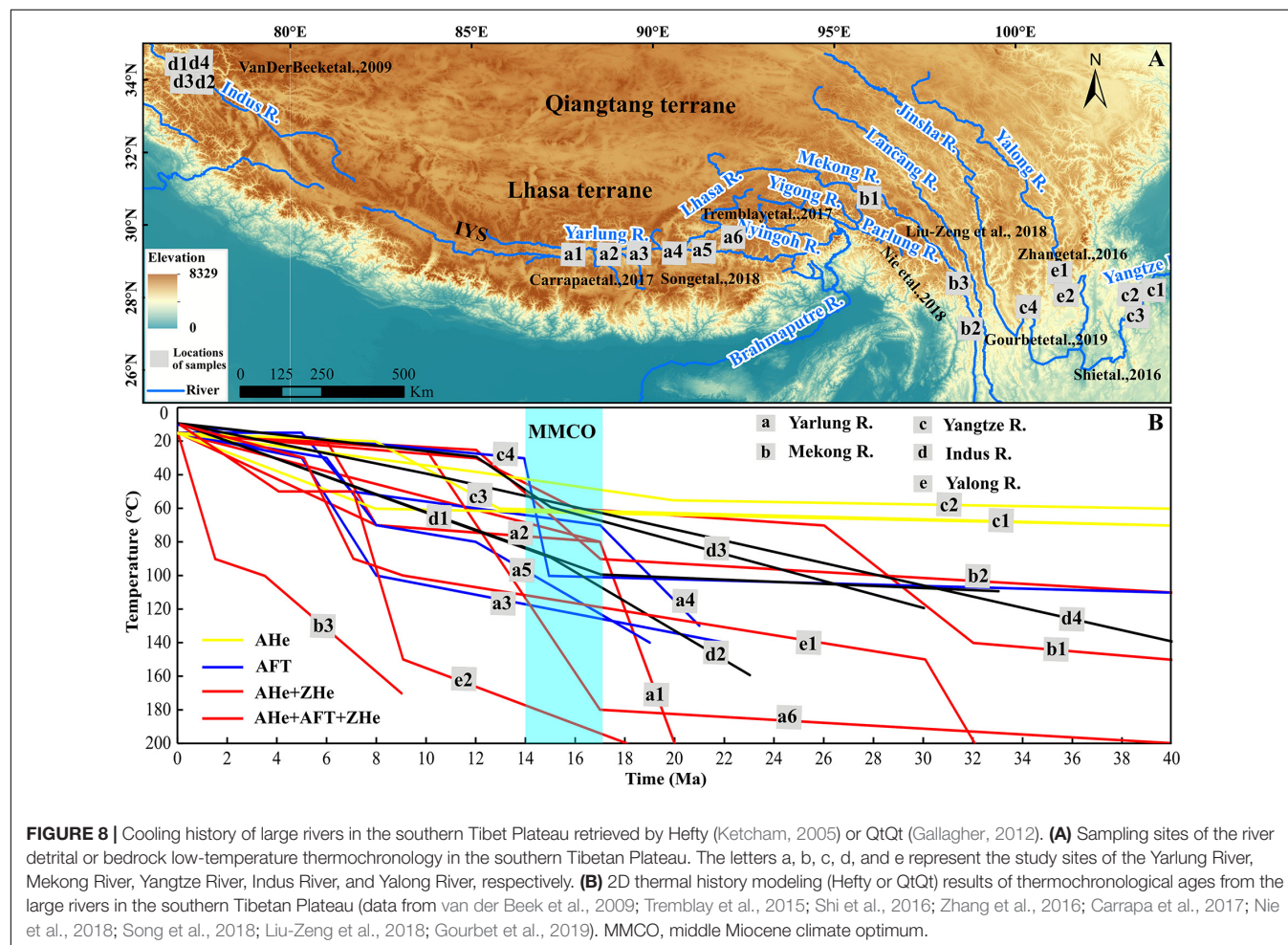
Moreover, we also compared the denudation rate with climate change (Figure 7B) and found that the rapid denudation in this stage also corresponds to the intensification of the Asian monsoon. Recent studies have shown that climatic change (precipitation or glacier development) determines the denudation of a large-scale area (Montgomery et al., 2001; Clift et al., 2008), but the orogenic tectonics could only trigger the erosion of the relatively local region (Beaumont et al., 2001; Luszczak et al., 2018; Yang et al., 2019; Shen et al., 2019). Based on this hypothesis, we have summarized the cooling history of five large rivers in the southeastern Tibetan Plateau from ~40 Ma to the present to identify the possible effect of climate on the denudation (Figure 8). This result suggests that not all rivers on the southeastern Tibetan Plateau underwent a rapid cooling at this period (Figure 8B), indicating that the rapid denudation at this stage is not dominated by climate, which further validates our viewpoint.

The Gangdese Thrust leads to the further uplift of the Gangdese Mountains, which could cut off the external paleodrainage from north to south in the southern Tibetan Plateau (Zhang et al., 2012; Han et al., 2019). At the same time, the southward paleodrainage in the southern Gangdese Mountains also rapidly incised in response to the uplift of the

Gangdese Mountains, leading to the formation of the initial Lhasa River. In the early Miocene, the development of the GCT system caused the uplift of the southern terranes (the Xigaze forearc basin, YTSZ, and Tethyan Himalaya) that might block the originally southward paleoflows (Wang et al., 2013; Li et al., 2018). The westward-flowing paleo-Yarlung River initiated at ~22 Ma (Wang et al., 2013) and captured the initial paleo-Lhasa River, possibly leading to the formation of the so-called barbed junction with southwestward-flowing tributaries (modern Lhasa River) of the Yarlung River (Figure 2). Theoretically, the formation of the modern Lhasa River will definitely lead to an increase in topographic relief, but the result of our simulation suggests that the topographic relief did not change significantly with the increase of denudation during this stage (Figure 7). This is probably related to the overall uplift of the central Gangdese Mountains during this phase due to the development of the GT and GCT (Figure 7A).

The Middle Miocene

Although previous studies have generally estimated a rapid denudation stage of the Gangdese region at ~23–0 or 20–10 Ma (Dai et al., 2013; Li et al., 2016; Ge et al., 2017), our modeling shows that a period of intense denudation existed



at ~ 15.5 – 12.3 Ma (with a rate of 0.72 km/Ma) (**Figure 7C**). The topographic relief in Lhasa River drainage also increased significantly (**Figure 7C**). An important climate event, the middle Miocene climate optimum (MMCO, ~ 17 – 14 Ma) happened, which is characterized by the warmest climate and highest atmospheric CO_2 concentrations during this period (Zachos et al., 2001; Tripathi et al., 2009). The MMCO corresponds to a phase of enhanced East and South Asian summer monsoon precipitation with large amplitude variability as recorded by offshore Southeastern Asian sediment accumulation rates (Clift, 2006; Yang et al., 2020). Meanwhile, the activity of the south-dipping GCT caused uplift and denudation of the Xigaze forearc basin, YTSZ, and Tethyan Himalaya in the southernmost Lhasa terrane (Wang et al., 2013; Li Y. L. et al., 2015). However, the middle reach of the Lhasa River is close to the central Lhasa terrane, and the tectonic activity of GCT should have a little impact on the denudation of the Lhasa River. Thus, we suggest that the intense denudation in this stage is more likely to be related to the large increasing Asian summer monsoon precipitation.

Furthermore, the cooling history of five large rivers in the southeastern Tibetan Plateau also underwent rapid cooling at this stage (**Figure 8B**), and this spatially large-scale synchronous rapid denudation including in the Lhasa River drainage should be dominated by climate (Montgomery et al., 2001; Clift et al., 2008). This is consistent with the fast incision of the Lhasa River, which leads to the topographic relief to increase rapidly ($R3 = 1.6$), which resulted in a relatively high-relief landscape (**Figure 7C**).

After ~ 12 Ma

The denudation rate and relief in the Lhasa River drainage significant decreased after ~ 12 Ma. The geological evidence suggested that the Himalaya experienced significant rock uplift since the late Miocene (**Figure 7**, e.g., MBT and MFT); thus, the orographic barrier to precipitation in the southern Tibetan Plateau would have strengthened (Tremblay et al., 2015), but the Lhasa River valley could be the only access for moisture penetration to the north and the precipitation decreased here. Therefore, the denudation rate significantly decreased. Another possibility was that a stationary knickzone results from coupling between focused rock uplift and rapidly fluvial incision within the Namche Barwa Syntaxis during the late Miocene (Lang and Huntington, 2014; Zeitler et al., 2014), creating a high-elevation base level for the drainage network upstream which inhabited the incision of the upper reaches of the Yarlung River. The decreasing of incision and low transport capacity in the upper Lhasa River might have led to the accumulation of the Lhasa River and reduced the topographic relief.

CONCLUSION

Based on a set of thermochronological ages reported in the Lhasa River valley, we have used a 3D thermokinematic model to carefully quantify rates and transition time of denudation under different scenarios. Two-stage rapid denudation rates at ~ 25 – 16 Ma (with a rate of 0.42 km/Ma) and ~ 16 – 12 Ma

(with a rate of 0.72 km/Ma) are revealed. Furthermore, the results of the drainage denudation history were combined with the data of topographic evolution to distinguish the tectonic and climate controls on geomorphic evolution of the Lhasa River drainage. The rapid denudation of the first phase (~ 25 – 16 Ma) could be caused by the activity of the Gangdese Thrust, which led to the overall uplift of the Gangdese Mountains. This might result in the reorganization of southward paleodrainage in the southern Tibetan Plateau, and the modern Lhasa River started to develop. The second stage of the fast denudation and high relief which correspond to a ubiquitous increase of fluvial incision in the southern Tibetan Plateau should be related to enhanced Asian summer monsoon precipitation during the middle Miocene. After that, the denudation rate decreased rapidly due to the uplift of the Himalayas barrier to precipitation, and a low-relief landscape gradually developed in the Gangdese region.

DATA AVAILABILITY STATEMENT

The original contributions presented in the study are included in the article/**supplementary material**, further inquiries can be directed to the corresponding author/s.

AUTHOR CONTRIBUTIONS

DC built the 3D model and wrote the first draft of the text. XW and GL guided the overarching research direction and advised on the interdisciplinary context. WZ advised on the geology. HL advised on the climatology. All authors contributed to the revision of the text.

FUNDING

This research is supported by the Second Tibetan Plateau Scientific Expedition Program (STEP) (2019QZKK0205; 2019QZKK2304), the National Natural Science Foundation of China (41971005), and the National Key Research and Development Program (grant number 2016YFA0600500).

ACKNOWLEDGMENTS

Thanks to Yang Yu, Qiang Su, and Zhengchen Li for their suggestions in writing. Jean Braun is thanked for providing the Pecube code. We also thank the reviewers RJ and JD for their helpful suggestions to improve the manuscript and editor GR for professional editorial handling.

SUPPLEMENTARY MATERIAL

The Supplementary Material for this article can be found online at: <https://www.frontiersin.org/articles/10.3389/feart.2021.636459/full#supplementary-material>

REFERENCES

- Ahnert, F. (1970). Functional relationships between denudation, relief, and uplift in large mid-latitude drainage basins. *Am. J. Sci.* 268, 243–263. doi: 10.2475/ajs.268.3.243
- Beaumont, C., Jamieson, R. A., Nguyen, M. H., and Lee, B. (2001). Himalayan tectonics explained by extrusion of a low-viscosity crustal channel coupled to focused surface denudation. *Nature* 414, 738–742. doi: 10.1038/414738a
- Beek, P. A. V. D., Valla, P. G., Herman, F., Braun, J., Persano, C., Dobson, K. J., et al. (2010). Inversion of thermochronological age-elevation profiles to extract independent estimates of denudation and relief history - I: theory and conceptual model. *Earth Planet. Sci. Lett.* 296, 9–22. doi: 10.1016/j.epsl.2010.04.032
- Bookhagen, B., and Burbank, D. W. (2010). Toward a complete Himalayan hydrological budget: spatiotemporal distribution of snowmelt and rainfall and their impact on river discharge. *J. Geophys. Res. Earth Surf.* 115:F03019. doi: 10.1029/2009JF001426
- Bookhagen, B., Thiede, R. C., and Strecker, M. R. (2005). Late Quaternary intensified monsoon phases control landscape evolution in the northwest Himalaya. *Geology* 33, 149–152. doi: 10.1130/G20982.1
- Braun, J. (2002). Quantifying the effect of recent relief changes on age–elevation relationships. *Earth Planet. Sci. Lett.* 200, 331–343. doi: 10.1016/S0012-821X(02)00638-6
- Braun, J. (2003). Pecube: a new finite-element code to solve the 3D heat transport equation including the effects of a time-varying, finite amplitude surface topography. *Comput. Geosci.* 29, 787–794. doi: 10.1016/S0098-3004(03)00052-9
- Braun, J., van der Beek, P., Valla, P., Robert, X., Herman, F., and Glotzbach, C. (2012). Quantifying rates of landscape evolution and tectonic processes by thermochronology and numerical modeling of crustal heat transport using PECUBE. *Tectonophysics* 524, 1–28. doi: 10.1016/j.tecto.2011.12.035
- Carrapa, B., Mohd, F., Kapp, P. A., Decelles, P. G., and Gehrels, G. (2017). Tectonic and erosional history of southern Tibet recorded by detrital chronological signatures along the yarlung river drainage. *Geol. Soc. Am. Bull.* 129, 570–581. doi: 10.1130/B31587.1
- Carrapa, B., Orme, D. A., Decelles, P. G., Kapp, P., Cosca, M. A., and Waldrip, R. (2014). Miocene burial and exhumation of the India-Asia collision zone in southern Tibet: response to slab dynamics and erosion. *Geology* 42, 443–446. doi: 10.1130/G35350.1
- Clift, P. D. (2006). Controls on the erosion of Cenozoic Asia and the flux of clastic sediment to the ocean. *Earth Planet. Sci. Lett.* 241, 571–580. doi: 10.1016/j.epsl.2005.11.028
- Clift, P. D., Hodges, K. V., Heslop, D., Hannigan, R., Van Long, H., and Calves, G. (2008). Correlation of Himalayan exhumation rates and Asian monsoon intensity. *Nat. Geosci.* 1, 875–880. doi: 10.1038/ngeo351
- Copeland, P., Harrison, T. M., Pan, Y., Kidd, W. S. F., Roden, M., and Zhang, Y. (1995). Thermal evolution of the Gangdese batholith, southern Tibet: a history of episodic unroofing. *Tectonics* 14, 223–236. doi: 10.1029/94TC01676
- Dai, J. G., Wang, C. S., Hourigan, J., Li, Z. J., and Zhuang, G. S. (2013). Exhumation history of the Gangdese batholith, Southern Tibetan Plateau: evidence from Apatite and Zircon (U-Th)/He thermochronology. *J. Geol.* 121, 155–172. doi: 10.1086/669250
- Davis, D., Suppe, J., and Dahlen, F. A. (1983). Mechanics of fold-and-thrust belts and accretionary wedges. *J. Geophys. Res.* 88, 1153–1172. doi: 10.1029/JB088iB02p01153
- DeCelles, P. G., Quade, J., Kapp, P., Fan, M. J., Dettman, D. L., and Ding, L. (2007). High and dry in central Tibet during the Late Oligocene. *Earth Planet. Sci. Lett.* 253, 389–401. doi: 10.1016/j.epsl.2006.11.001
- Ding, L., Xu, Q., Yue, Y. H., Wang, H. Q., Cai, F. L., and Li, S. (2014). The andean-type gangdese mountains: paleoelevation record from the paleocene-eocene linzhou basin. *Earth Planet. Sci. Lett.* 392, 250–264. doi: 10.1016/j.epsl.2014.01.045
- Ehlers, T. A. (2005). Crustal thermal processes and the interpretation of thermochronometer data. *Low Temp. Thermochronol.* 58, 315–350. doi: 10.2138/rmg.2005.58.12
- England, P., and Molnar, P. (1990). Surface uplift, uplift of rocks, and exhumation of rocks. *Geology* 18, 1173–1177.
- Gadgil, S. (2003). The Indian monsoon and its variability. *Annu. Rev. Earth Planet. Sci.* 31, 429–467. doi: 10.1146/annurev.earth.31.100901.141251
- Gallagher, K. (2012). Transdimensional inverse thermal history modeling for quantitative thermochronology. *J. Geophys. Res. Solid Earth* 117:B02408. doi: 10.1029/2011JB008825
- Gallagher, K., Stephenson, J., Brown, R., Holmes, C., and Ballester, P. (2005a). Exploiting 3D spatial sampling in inverse modeling of thermochronological data. *Low Temp. Thermochronol.* 58, 375–387. doi: 10.2138/rmg.2005.58.14
- Gallagher, K., Stephenson, J., Brown, R., Holmes, C., and Fitzgerald, P. (2005b). Low temperature thermochronology and modeling strategies for multiple samples I: vertical profiles. *Earth Planet. Lett.* 237, 193–208. doi: 10.1016/j.epsl.2005.06.025
- Ge, Y. K., Dai, J. G., Wang, C. S., Li, Y. L., Xu, G. Q., and Danisik, M. (2017). Cenozoic thermo-tectonic evolution of the Gangdese batholith constrained by low-temperature thermochronology. *Gondwana Res.* 41, 451–462. doi: 10.1016/j.jgr.2016.05.006
- Gourbet, L., Yang, R., Fellin, M. G., Paquette, J. L., Willett, S. D., Gong, J. F., et al. (2019). Evolution of the yangtze river network, southeastern tibet: insights from thermochronology and sedimentology. *Lithosphere* 12, 3–18. doi: 10.1130/L1104.1
- Han, Z. P., Sinclair, H. D., Li, Y. L., Wang, C. S., Tao, Z., and Qian, X. Y. (2019). Internal drainage has sustained low-relief tibetan landscapes since the early miocene. *Geophys. Res. Lett.* 46, 8741–8752. doi: 10.1029/2019GL083019
- Harrison, T. M., Copeland, P., Kidd, W. S. F., and Yin, A. (1992). Raising Tibet. *Science* 255, 1663–1670. doi: 10.1126/science.255.5052.1663
- Harrison, T. M., Yin, A., Grove, M., Lovera, O. M., Ryerson, F. J., and Zhou, X. H. (2000). The Zedong Window: a record of superposed Tertiary convergence in southeastern Tibet. *J. Geophys. Res. Solid Earth* 105, 19211–19230. doi: 10.1029/2000JB900078
- Hetzl, R., Dunkl, I., Haider, V., Strobl, M., von Eynatten, H., Ding, L., et al. (2011). Peneplain formation in southern Tibet predates the India-Asia collision and plateau uplift. *Geology* 39, 983–986. doi: 10.1130/g34504y.1
- Ji, W. Q., Wu, F. Y., Chung, S. L., Li, J. X., and Liu, C. Z. (2009). Zircon U-Pb geochronology and Hf isotopic constraints on petrogenesis of the Gangdese batholith, southern Tibet. *Chem. Geol.* 262, 229–245. doi: 10.1016/j.chemgeo.2009.01.020
- Ketchum, R. A. (2005). Forward and inverse modeling of low-temperature thermochronometry data. *Rev. Mineral. Geochem.* 58, 275–314. doi: 10.2138/rmg.2005.58.11
- Khan, M. A., Bera, M., Spicer, R. A., Spicer, T. E. V., and Bera, S. (2019). Palaeoclimatic estimates for a latest Miocene-Pliocene flora from the Siwalik Group of Bhutan: Evidence for the development of the South Asian Monsoon in the eastern Himalaya. *Palaeogeogr. Palaeoclimatol. Palaeoecol.* 514, 326–335. doi: 10.1016/j.palaeo.2018.10.019
- Lang, K. A., and Huntington, K. W. (2014). Antecedence of the Yarlung-Siang-Brahmaputra River, eastern Himalaya. *Earth Planet. Sci. Lett.* 397, 145–158. doi: 10.1016/j.epsl.2014.04.026
- Laskowski, A. K., Orme, D. A., Cai, F. L., and Ding, L. (2019). The Ancestral Lhasa River: a late cretaceous trans-arc river that drained the proto-Tibetan Plateau. *Geology* 47, 1029–1033. doi: 10.1130/G46823.1
- Li, G. W., Kohn, B., Sandiford, M., Ma, Z. L., and Xu, Z. Q. (2018). Post-collisional exhumation of the Indus-Yarlung suture zone and Northern Tethyan Himalaya, Saga, SW Tibet. *Gondwana Res.* 64, 1–10.
- Li, G. W., Kohn, B., Sandiford, M., Xu, Z. Q., Tian, Y. T., and Seiler, C. (2016). Synorogenic morphotectonic evolution of the Gangdese batholith, South Tibet: Insights from low-temperature thermochronology. *Geochem. Geophys. Geosyst.* 17, 101–112. doi: 10.1002/2015GC006047
- Li, G. W., Tian, Y. T., Kohn, B. P., Sandiford, M., Xu, Z. Q., and Cai, Z. H. (2015). Cenozoic low temperature cooling history of the Northern Tethyan Himalaya in Zedang, SE Tibet and its implications. *Tectonophysics* 643, 80–93. doi: 10.1016/j.tecto.2014.12.014
- Li, S., Ding, L., Xu, Q., Wang, H. Q., Yue, Y. H., and Baral, U. (2017). The evolution of Yarlung Tsangpo River: constraints from the age and provenance of the Gangdese Conglomerates, southern Tibet. *Gondwana Res.* 41, 249–266. doi: 10.1016/j.jgr.2015.05.010

- Li, Y. L., Wang, C. S., Dai, J. G., Xu, G. Q., Hou, Y. L., and Li, X. H. (2015). Propagation of the deformation and growth of the Tibetan-Himalayan orogen: a review. *Earth Sci. Rev.* 143, 36–61. doi: 10.1016/j.earscirev.2015.01.001
- Liu-Zeng, J., Zhang, J. Y., McPhillips, D., Reiners, P., Wei, W., and Pik, R. (2018). Multiple episodes of fast exhumation since Cretaceous in southeast Tibet, revealed by low-temperature thermochronology. *Earth Planet. Sci. Lett.* 490, 62–76. doi: 10.1016/j.epsl.2018.03.011
- Luszczak, K., Persano, C., Braun, J., and Stuart, F. M. (2018). How local crustal thermal properties influence the amount of denudation derived from low-temperature thermochronometry. *Geology* 46, E439–E439. doi: 10.1130/G39036.1
- McDannell, K. T., Zeitler, P. K., and Idleman, B. D. (2018). Relict topography within the Hangay mountains in Central Mongolia: quantifying long-term exhumation and relief change in an old landscape. *Tectonics* 37, 2531–2558. doi: 10.17605/OSF.IO/BPHYS
- Mo, X. X., Niu, Y. L., Dong, G. C., Zhao, Z. D., Hou, Z. Q., Zhou, S., et al. (2008). Contribution of syncollisional felsic magmatism to continental crust growth: a case study of the Paleogene Linzizong volcanic Succession in southern Tibet. *Chem. Geol.* 250, 49–67. doi: 10.1016/j.chemgeo.2008.02.003
- Molnar, P., Boos, W. R., and Battisti, D. S. (2010). Orographic controls on climate and paleoclimate of Asia: thermal and mechanical roles for the Tibetan Plateau. *Annu. Rev. Earth Planet. Sci.* 38, 77–102. doi: 10.1146/annurev-earth-040809-152456
- Montgomery, D. R., Balco, G., and Willett, S. D. (2001). Climate, tectonics, and the morphology of the Andes. *Geology* 29, 579–582. doi: 10.1130/0091-7613(2001)0292.0.CO;2
- Naito, N., Ageta, Y., Iwata, S., Matsuda, Y., Suzuki, R., Karma, et al. (2006). Glacier shrinkages and climate conditions around Jichu Dramo Glacier in the Bhutan Himalayas from 1998 to 2003. *Bull. Glaciol. Res.* 23, 51–61. doi: 10.1007/s11407-999-0013-0
- Nie, J. S., Ruetenik, G., Gallagher, K., Hoke, G., Garziona, C. N., and Wang, W. T. (2018). Rapid incision of the Mekong River in the middle Miocene linked to monsoonal precipitation. *Nat. Geosci.* 11, 944–948. doi: 10.1038/s41561-018-0244-z
- Pan, B. T., Burbank, D., Wang, Y. X., Wu, G. J., Li, J. J., and Guan, Q. Y. (2003). A 900 ky record of strath terrace formation during glacial-interglacial transitions in northwest China. *Geology* 31, 957–960. doi: 10.1130/G19685.1
- Rowley, D. B., and Currie, B. S. (2006). Palaeo-altimetry of the late Eocene to Miocene Lunpola basin, central Tibet. *Nature* 439, 677–681. doi: 10.1038/nature04506
- Sambridge, M. (2010a). Geophysical inversion with a neighbourhood algorithm—I. Searching a parameter space. *Geophys. J. R. Astron. Soc.* 138, 479–494. doi: 10.1046/j.1365-246X.1999.00876.x
- Sambridge, M. (2010b). Geophysical inversion with a neighbourhood algorithm—II. Appraising the ensemble. *Transl. World Ssmol.* 138, 727–746. doi: 10.1046/j.1365-246x.1999.00900.x
- Schildgen, T. F., Ehlers, T. A., Whipp, D. M., van Soest, M. C., Whipple, K. X., and Hodges, K. V. (2009). Quantifying canyon incision and Andean Plateau surface uplift, southwest Peru: a thermochronometer and numerical modeling approach. *J. Geophys. Res. Earth Surf.* 114:F04014. doi: 10.1029/2009JF001305
- Shen, X. M., Tian, Y. T., Zhang, G. H., Zhang, S. M., Carter, A., and Kohn, B. (2019). Late miocene hinterland crustal shortening in the longmen shan thrust belt, the eastern margin of the Tibetan Plateau. *J. Geophys. Res. Solid Earth* 124, 11972–11991. doi: 10.1029/2019JB018358
- Shi, H. C., Shi, X. B., Glasmacher, U. A., Yang, X. Q., and Stockli, D. F. (2016). The evolution of eastern Sichuan basin, Yangtze block since Cretaceous: constraints from low temperature thermochronology. *J. Asian Earth Sci.* 116, 208–221. doi: 10.1016/j.jseas.2015.11.008
- Song, S. Y., Cao, D. Y., Zhang, Q. C., Wang, A. M., and Peng, Y. W. (2018). Apatite fission track evidence for Miocene denudation history in the Gangdese conglomerate belt and Yarlung Tsangpo River: Implications for the evolution of Southern Tibet. *J. Asian Earth Sci.* 160, 159–167. doi: 10.1016/j.jseas.2018.04.021
- Tian, Y. T., Kohn, B. P., Gleadow, A. J. W., and Hu, S. B. (2013). Peneplain formation in southern Tibet predates the India-Asia collision and plateau uplift Comment. *Geology* 41, E295–E296. doi: 10.1130/G33617C.1
- Tian, Y. T., Kohn, B. P., Hu, S. B., and Gleadow, A. J. W. (2015). Synchronous fluvial response to surface uplift in the eastern Tibetan Plateau: implications for crustal dynamics. *Geophys. Res. Lett.* 42, 29–35. doi: 10.1002/2014GL062383
- Tremblay, M. M., Fox, M., Schmidt, J. L., Tripathy-Lang, A., Wielicki, M. M., Harrison, T. M., et al. (2015). Erosion in southern Tibet shut down at similar to 10 Ma due to enhanced rock uplift within the Himalaya. *Proc. Natl. Acad. Sci. U.S.A.* 112, 12030–12035. doi: 10.1073/pnas.1515652112
- Tripathi, A. K., Roberts, C. D., and Eagle, R. A. (2009). Coupling of CO₂ and ice sheet stability over major climate transitions of the last 20 million years. *Science* 326, 1394–1397. doi: 10.1126/science.1178296
- Valla, P. G., Herman, F., van der Beek, P. A., and Braun, J. (2010). Inversion of thermochronological age-elevation profiles to extract independent estimates of denudation and relief history - I: Theory and conceptual model. *Earth Planet. Sci. Lett.* 295, 511–522. doi: 10.1016/j.epsl.2010.04.032
- van der Beek, P., Van Melle, J., Guillot, S., Pecher, A., Reiners, P. W., Nicolescu, S., et al. (2009). Eocene Tibetan plateau remnants preserved in the northwest Himalaya. *Nat. Geosci.* 2, 364–368. doi: 10.1038/ngeo503
- Wang, F., Feng, H., Shi, W., Zhang, W., Wu, L., Yang, L., et al. (2016). Relief history and denudation evolution of the northern Tibet margin: constraints from 40Ar/39Ar and (U–Th)/He dating and implications for far-field effect of rising plateau. *Tectonophysics* 675, 196–208. doi: 10.1016/j.tecto.2016.03.001
- Wang, J. G., Hu, X. M., Garzanti, E., and Wu, F. Y. (2013). Upper oligocene-lower miocene gangrinboche conglomerate in the Xigaze area, Southern Tibet: implications for Himalayan Uplift and Paleo-Yarlung-Zangbo initiation. *J. Geol.* 121, 425–444.
- Wang, P. X., Wang, B., Cheng, H., Fasullo, J., Guo, Z. T., Kiefer, T., et al. (2017). The global monsoon across time scales: mechanisms and outstanding issues. *Earth Sci. Rev.* 174, 84–121.
- Wang, X. Y., Lu, H. Y., Vandenberghe, J., Zheng, S. H., and van Balen, R. (2012). Late Miocene uplift of the NE Tibetan Plateau inferred from basin filling, planation and fluvial terraces in the Huang Shui catchment. *Glob. Planet. Change* 88–89, 10–19. doi: 10.1016/j.gloplacha.2012.02.009
- Wang, X. Y., Vandenberghe, J., Yi, S. W., Van Balen, R., and Lu, H. Y. (2015). Climate-dependent fluvial architecture and processes on a suborbital timescale in areas of rapid tectonic uplift: an example from the NE Tibetan Plateau. *Glob. Planet. Change* 133, 318–329. doi: 10.1016/j.gloplacha.2015.09.009
- Wei, L. G., Sandiford, M., Liu, X. H., Xu, Z. Q., Wei, L. J., and Li, H. Q. (2014). Provenance of Late Triassic sediments in central Lhasa terrane, Tibet and its implication. *Gondwana Res.* 25, 1680–1689. doi: 10.1016/j.gr.2013.06.019
- Whipp, D. M. Jr., Ehlers, T. A., Blythe, A. E., Huntington, K. W., Hodges, K. V., and Burbank, D. W. (2007). Plio-Quaternary exhumation history of the central Nepalese Himalaya: 2. Thermokinematic and thermochronometer age prediction model. *Tectonics* 26:TC3003. doi: 10.1029/2006TC001991
- Whipple, K. X. (2009). The influence of climate on the tectonic evolution of mountain belts (vol 2, pg 97, 2009). *Nat. Geosci.* 2, 730–730. doi: 10.1038/ngeo413
- Whipple, K. X., Hancock, G. S., and Anderson, R. S. (2000). River incision into bedrock: Mechanics and relative efficacy of plucking, abrasion, and cavitation. *Geol. Soc. Am. Bull.* 112, 490–503. doi: 10.1130/0016-7606(2000)1122.0.CO;2
- Wilson, C. J. L., and Fowler, A. P. (2011). Denudational response to surface uplift in east Tibet: evidence from apatite fission-track thermochronology. *Geol. Soc. Am. Bull.* 123, 1966–1987. doi: 10.1130/B30331.1
- Yang, R., Herman, F., and Fellin, M. G. (2019). Exhumation and topographic evolution of the Namche Barwa Syntaxis, eastern Himalaya. *Tectonophysics* 722, 43–52. doi: 10.1016/j.tecto.2017.10.026
- Yang, X. P., Groenewald, J., Jian, Z. M., Steinke, S., and Giosan, L. (2020). Middle miocene intensification of South Asian Monsoonal Rainfall. *Paleoceanogr. Paleoclimatol.* 35, 1–18. doi: 10.1029/2020PA003853
- Yin, A., and Harrison, T. M. (2000). Geologic evolution of the Himalayan-Tibetan orogen. *Annu. Rev. Earth Planet. Sci.* 28, 211–280. doi: 10.1146/annurev.earth.28.1.211
- Yin, A., Harrison, T. M., Murphy, M. A., Grove, M., Nie, S., and Ryerson, F. J. (1999). Tertiary deformation history of southeastern and southwestern Tibet during the Indo-Asian collision. *Geol. Soc. Am. Bull.* 111, 1644–1664. doi: 10.1130/0016-7606(1999)1112.3.CO;2
- Yin, A., Harrison, T. M., Ryerson, F. J., Chen, W. J., Kidd, W. S. F., and Copeland, P. (1994). Tertiary structural evolution of the Gangdese Thrust

- System, Southeastern Tibet. *J. Geophys. Res. Solid Earth* 99, 18175–18201. doi: 10.1029/94JB00504
- Zachos, J., Pagani, M., Sloan, L., Thomas, E., and Billups, K. (2001). Trends, rhythms, and aberrations in global climate 65 Ma to present. *Science* 292, 686–693. doi: 10.1126/science.1059412
- Zeitler, P. K., Meltzer, A. S., Brown, L., Kidd, W. S. F., Lim, C., and Enkelmann, E. (2014). “Tectonics and topographic evolution of Namche Barwa and the easternmost Lhasa block, Tibet,” in *Toward an Improved Understanding of Uplift Mechanisms and the Elevation History of the Tibetan Plateau*, eds J. Nie, B. K. Horton, and G. D. Hoke (Boulder, CO: Geological Society of America), 23–58. doi: 10.1130/2014.2507(02)
- Zeitler, P. K., Meltzer, A. S., Koons, P. O., Craw, D., Hallet, B., Chamberlain, C. P., et al. (2001). Erosion, Himalayan geodynamics, and the geomorphology of metamorphism. *GSA Today* 11, 4–9. doi: 10.1130/1052-5173(2001)0112.0.CO;2
- Zhang, H. P., Oskin, M. E., Liu-Zeng, J., Zhang, P. Z., Reiners, P. W., and Xiao, P. (2016). Pulsed exhumation of interior eastern Tibet: implications for relief generation mechanisms and the origin of high-elevation planation surfaces. *Earth Planet. Sci. Lett.* 449, 176–185. doi: 10.1016/j.epsl.2016.05.048
- Zhang, J. Y., Yin, A., Liu, W. C., Wu, F. Y., Lin, D., and Grove, M. (2012). Coupled U-Pb dating and Hf isotopic analysis of detrital zircon of modern river sand from the Yalu River (Yarlung Tsangpo) drainage system in southern Tibet: constraints on the transport processes and evolution of Himalayan rivers. *Geol. Soc. Am. Bull.* 124, 1449–1473. doi: 10.1130/B30592.1
- Zhang, P. Z., Peter, M., and William, R. W. (2001). Increased sedimentation rates and grain sizes 2–4 Myr ago due to the influence of climate change on erosion rates. *Nature* 410, 891–897. doi: 10.1038/35073504
- Zhu, D. C., Zhao, Z. D., Niu, Y. L., Mo, X. X., Chung, S. L., and Hou, Z. Q. (2011). The Lhasa Terrane: record of a microcontinent and its histories of drift and growth. *Earth Planet. Sci. Lett.* 301, 241–255. doi: 10.1016/j.epsl.2010.11.005
- Conflict of Interest:** The authors declare that the research was conducted in the absence of any commercial or financial relationships that could be construed as a potential conflict of interest.
- Copyright © 2021 Cai, Wang, Li, Zhu and Lu. This is an open-access article distributed under the terms of the Creative Commons Attribution License (CC BY). The use, distribution or reproduction in other forums is permitted, provided the original author(s) and the copyright owner(s) are credited and that the original publication in this journal is cited, in accordance with accepted academic practice. No use, distribution or reproduction is permitted which does not comply with these terms.